IOP Publishing Semiconductor Science and Technology
Semicond. Sci. Technol. **31** (2016) 105015 (8pp) doi:10.1088/0268-1242/31/10/105015

Random networks of carbon nanotubes optimized for transistor mass-production: searching for ultimate performance

M Žeželj[1,2] and I Stanković[2]

[1] School of Electrical Engineering, University of Belgrade, Bulevar kralja Aleksandra 73, 11120 Belgrade, Serbia
[2] Scientific Computing Laboratory, Center for the Study of Complex Systems, Institute of Physics Belgrade, University of Belgrade, Pregrevica 118, 11080 Belgrade, Serbia

E-mail: igor.stankovic@ipb.ac.rs

Received 26 May 2016, revised 14 July 2016
Accepted for publication 26 July 2016
Published 19 September 2016

Abstract

Random networks of as-grown single-walled carbon nanotubes (CNTs) contain both metallic (m-CNTs) and semiconducting (s-CNTs) nanotubes in an approximate ratio of 1:2, which leads to a trade-off between on-conductance and the on/off ratio. We demonstrate how this design problem can be solved with a realistic numerical approach. We determine the CNT density, length, and channel dimensions under which CNT thin-film transistors simultaneously attain on-conductance higher than 1 μS and an on/off ratio higher than 10^4. The fact that asymmetric systems have more pronounced finite-size scaling behavior than symmetric systems allows us additional design freedom. A realization probability of the desired characteristics higher than 99% is obtained for the channels with aspect ratio $L_{CH}/W_{CH} < 1.2$ and normalized size $L_{CH}W_{CH}/l_{CNT}^2 > 250$ when the CNT length is $l_{CNT} = 4 - 20$ μm and the normalized density of CNTs is close to the value where the probability of percolation through only s-CNT pathways reaches its maximum.

S Online supplementary data available from stacks.iop.org/sst/31/105015/mmedia

Keywords: random network, carbon nanotubes, thin-film transistor, electrical conductance

(Some figures may appear in colour only in the online journal)

1. Introduction

Recently, random carbon nanotube (CNT) networks have been demonstrated as potential active materials in electronics applications [1], optoelectronics [2], sensors [3], and memory cells [4]. CNT thin-film transistors (TFTs) are expected to enable the fabrication of high-performance, flexible, and transparent devices using relatively simple techniques [5–14]. As-grown networks of single-walled (SW) CNTs contain both metallic (m-CNTs) and semiconducting (s-CNTs) nanotubes, which leads to a trade-off between on-conductance and the on/off conductance ratio [15–17]. If the density of CNTs in a TFT is sufficiently high that m-CNTs exceed the percolation threshold, the CNT network will become predominantly metallic and, hence, the on/off ratio will be very small. In contrast, if the CNT density is so low that a conduction path through the m-CNTs does not exist, a high on/off ratio can be attained, but under such circumstances the low on-conductance is a disadvantage [18].

Various experimental efforts have been made to increase both the on-conductance and on/off ratio of CNT TFTs. With roughly 1/3 of as-grown CNTs being metallic extra steps, such as selective removal of m-CNTs via an electrical breakdown method [19], they are used in order to cut the metallic paths through the transistors. However, such breakdown also removes some s-CNT pathways leading to a decrease of the on-conductance. If the breakdown is applied when the s-CNTs in the network are gated to the off-state, most of the s-CNTs will be well preserved and the on-conductance will not be affected much [4]. However, using

 © 2016 IOP Publishing Ltd Printed in the UK

additional steps after the CNT synthesis process, such as electrical breakdown methods, prolongs the production time and thus increases the production costs. Other researchers have used semiconducting enriched CNTs in order to enhance the performance of CNT TFTs. For example, methods which separate CNTs by electronic type, such us centrifugation of compositions of CNTs with surface active components in density-gradient media [20] or the gas-phase plasma hydrocarbonation reaction technique [21], are used after or during the CNT synthesis process. However, these techniques also create defects in the remaining CNT networks and add impurities, which degrade the overall performance of the TFTs [22–24]. This approach also increases the difficulty of the fabrication process, and the repeatability and uniformity of devices are uncertain [22].

The effects of m-CNTs in a random network can be reduced by carefully controlling the CNT density, length, and device geometry, such that the metallic fraction of the CNTs is below the percolation threshold [1], i.e. every conducting path contains at least one semiconducting CNT. An optimized device, i.e. the highest possible on-conductance at a given on/off ratio, has a total density of CNTs above the percolation threshold and a density of m-CNTs below the percolation threshold. Although such high quality devices have been reported in the literature [18, 25–27], numerical simulations and experiments to determine the CNT density, channel size, and CNT length for optimum device performance, fabricated at industrial yield rates, are lacking.

In this paper, we study the effects of the device parameters (density of CNTs, channel dimensions, and CNT length) on the electrical properties in order to obtain an optimized and uniform device performance without using any post-growth treatment. We identify the probabilities of different conduction regimes of random CNT networks based on our recently determined scaling laws for asymmetric systems of percolating sticks [28]. Finally, we demonstrate how geometrical aspects contribute to the feasibility of random CNT networks as switches with good transistor performance (i.e. high on-current and on/off ratio) and the uniform performance of realized devices.

2. Numerical method

Monte Carlo (MC) simulations are coupled with an efficient iterative algorithm implemented on the grid platform and are used to investigate the electrical properties of CNT networks [28–31]. We consider two-dimensional systems with isotropically placed CNTs modeled as width-less sticks with a fixed length l_{CNT}. The centers of the CNTs are randomly positioned and oriented inside a channel with length L_{CH} and width W_{CH}. Source and drain electrodes are placed at the left and right sides of the channel. The top and bottom boundaries of the system are free and nonconducting, because free boundary conditions are more consistent with CNT networks in practice. The behavior of the CNT network is studied in terms of the normalized CNT density $n = N/\mathcal{L}^2$, where N is the total number of CNTs and $\mathcal{L} = \sqrt{LW}$ is the normalized channel size, where $L = L_{CH}/l_{CNT}$ is the normalized channel length and $W = W_{CH}/l_{CNT}$ is the normalized channel width, see [32]. The aspect ratio of the system r is defined as the ratio of the channel length and width $r = L/W$, see [28]. Without elaborate post-growth treatments, the CNTs synthesized using any available method are heterogeneous in the sense that they are always a mixture of metallic and semiconducting nanotubes with an approximate ratio of 1:2, i.e. the fraction of m-CNTs is $f_M = 1/3$ and the rest are s-CNTs with the fraction $f_S = 2/3$ [23, 33].

We only consider long-channel limits ($L_{CH} > l_{CNT}$) consistent with macroelectronics [15] and low-bias conditions under which nonlinear effects are negligible [33]. For long-channel limits, conduction in the CNT network is described by percolation theory as being that of a non-classical two-dimensional conductor [29]. Two sticks (CNTs) belong to the same cluster if they intersect. The system percolates (conducts) if the electrodes (source and drain) are connected with the same cluster [34]. The percolation threshold of the infinite-size stick system is defined by the critical density $n_c \approx 5.64$ [28]. Similarly, the percolation threshold of only s-CNTs is defined by the critical density $n_c/f_S \approx 8.46$ and the percolation threshold of only m-CNTs is $n_c/f_M \approx 16.9$.

The conductance along a CNT segment in the on-state, G_{seg}, is assumed to be uniform and can be calculated using [26, 27, 35]

$$G_{seg} = \frac{4e^2}{h}\frac{\lambda}{\lambda + l_{seg}}, \tag{1}$$

where e is the electron charge, h is Planck's constant, l_{seg} is the length of the CNT segment, and λ is the mean free path of the electrons, which is taken as 1.0 μm for m-CNTs and 0.3 μm for s-CNTs [36–38]. We consider that the conductance of an m-CNT is independent of the gate voltage [33] and in the off-state is also given by equation (1). At the same time, we assume that the conductance of an s-CNT in the off-state is 10^6 times lower than in the on-state, since the on/off ratio is usually about 10^6 for well-performing transistors based on individual s-CNTs [39, 40]. We note here that in real systems, the gate dielectric and gate leakage also contribute to the off-current, and thus the on/off ratio. Equation (1) assumes diffusive electrical transport through the CNTs, typical for rodlike nanostructures whose length is larger than the mean free path of the electrons ($l_{CNT} \gg \lambda$). For the diffusive electrical transport the electrical conductance of a stick segment is inversely proportional to the length of the CNT segment $(4e^2/h)(\lambda/l_{seg})$, see [41, 42]. The conductance of a CNT whose length is lower than the mean free path of the electrons ($l_{CNT} \ll \lambda$) is near the ballistic transport limit $4e^2/h$ and also can be assumed by equation (1), see [36, 40].

Internal nodes for contacts between pairs of CNTs are distinguished from boundary nodes for contacts between CNTs and the source/drain electrodes. The contact conductances for the internal nodes are assigned the following values: (i) $0.1e^2/h$ for the junction between two m-CNTs or between two s-CNTs and (ii) 100 times lower conductance for the junction between one m-CNT and one s-CNT, since we neglect the rectifying behavior under low-bias conditions

[33, 43]. The contact resistance at the boundary nodes is neglected since electrodes fabricated using, for example, Au [1], Pd [40], or aligned arrays of m-CNTs [44] yield good Ohmic contact to CNTs. Therefore, if a CNT intersects an electrode the potential of the electrode is applied to the intersection point. Kirchhoff's current law was used to balance the current flow through each node of the created network. An iterative equation solver (i.e. conjugate gradient method with Jacobi preconditioner) has been employed to solve a large system of linear equations following from Kirchhoff's laws [29]. After obtaining the total source–drain current I under an applied voltage V the macroscopic electrical conductance of the system is evaluated as $G = I/V$.[3] Finally, for each set of system parameters, electrical conductances for the on- and off-state are calculated for more than 10^5 independent MC realizations for systems with normalized size $L = W = 2$, down to 10^4 realizations for the largest system $L = W = 50$ studied. The results obtained using our conductance model show excellent agreement with recently published experimental results, see the supplementary material, section 1. We note here that our conductance model can also be applied to random networks of multi-walled (MW) CNTs with a small diameter[4] and, with some modifications, to random networks of nanowires (NWs)[5].

3. Symmetric-channel results

The randomly generated CNT network, if conducting, belongs to one of three complementary CNT network regimes according to its percolation characteristics: (i) neither m-CNT nor s-CNT paths exist but the whole network percolates through a mixed path comprising m- and s-CNTs ($\overline{\mathrm{S}}\,\overline{\mathrm{M}}$), (ii) only s-CNT paths exist ($\mathrm{S}\overline{\mathrm{M}}$), and (iii) at least one m-CNT path exists (M).

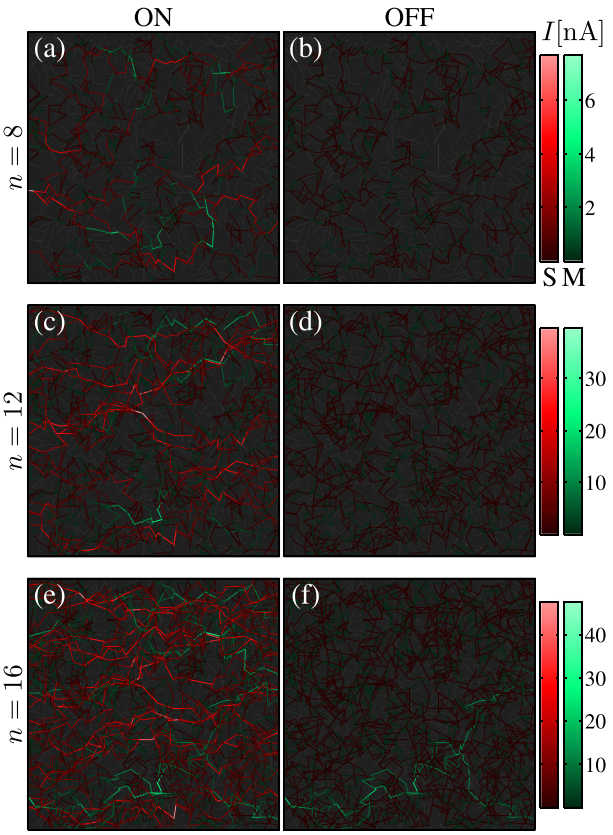

Figure 1. Simulated on- ((a), (c), and (e)) and off-current ((b), (d), and (f)) distributions for different CNT densities. The source–drain voltage is $V = 0.1$ V, the CNT length is $l_{\mathrm{CNT}} = 5$ μm, and the channel dimensions are $L_{\mathrm{CH}} = W_{\mathrm{CH}} = 50$ μm, i.e. the normalized system size is $L = 10$. (a) When the density of CNTs ($n = 8$) is significantly lower than the percolation threshold of only s-CNTs ($n < n_{\mathrm{c}}/f_{\mathrm{S}}$), the dominant percolation domain is through mixed paths comprising m- and s-CNTs ($\overline{\mathrm{S}}\,\overline{\mathrm{M}}$). (b) Since there is no percolating path through only m-CNTs the off-current is low, i.e. the on/off ratio is high. (c) For a higher CNT density ($n = 12$) only s-CNT paths exist ($\mathrm{S}\overline{\mathrm{M}}$), resulting in a high on-current I_{ON}. (d) This CNT density ($n = 12$) is still lower than the percolation threshold of only m-CNTs and, therefore, the CNT TFT is not short-circuited in the off-state and the on/off ratio is still high. (e) For high CNT density ($n = 16$) the m-CNT network percolates. (f) The CNT network in the off-state is shorted through the m-CNTs.

Figure 1 illustrates the structure of the CNT networks and the redistribution of the currents in on- and off-states with increasing CNT density n. When the CNT density n increases the randomly generated CNT network moves from one operation regime to another. The first regime ($\overline{\mathrm{S}}\,\overline{\mathrm{M}}$) corresponds to a situation when the density of CNTs ($n = 8$) is higher than the percolation threshold of the entire network n_{c} but lower than the percolation threshold of only s-CNTs ($n_{\mathrm{c}} < n < n_{\mathrm{c}}/f_{\mathrm{S}}$). In this situation the percolating network consists of mixed m- and s-CNTs. As a result, the

[3] The on/off ratio is defined as the ratio of the on- and off-state currents determined at the same source–drain voltage V, i.e. $I_{\mathrm{ON}}/I_{\mathrm{OFF}}$. We only consider low-bias conditions, i.e. $V \approx 0$, under which nonlinear effects are negligible and the currents are given by $I_{\mathrm{ON}} = G_{\mathrm{ON}}V$ and $I_{\mathrm{OFF}} = G_{\mathrm{OFF}}V$, respectively. Hence, the on/off current ratio $I_{\mathrm{ON}}/I_{\mathrm{OFF}}$ is equal to the on/off conductance ratio, i.e. $G_{\mathrm{ON}}/G_{\mathrm{OFF}}$.

[4] SW CNTs have the smallest diameter of all CNTs, distributed within a narrow range ($d_{\mathrm{CNT}} = 0.8 - 5$ nm), and a length l_{CNT} from tens of nanometers to millimeters, whereas MW CNTs have a larger diameter (~3 to > 100 nm) and lengths similar to those of SW CNTs, as noted in [13]. Our scaling model for systems of percolating sticks, which describes the operation regimes of random CNT TFTs, is valid for both SW and MW CNT networks as long as the CNTs can be modeled as width-less sticks, i.e. $l_{\mathrm{CNT}}/d_{\mathrm{CNT}} \gg 1$. On the other hand, the electrical characteristics of individual CNTs are primarily determined by their band gap [13]. It is well known that the band gap of an s-CNT depends inversely on its diameter. However, this dependence is not highly pronounced in the case of SW CNTs, since they have small diameters, distributed within a narrow range [13]. Therefore, our conductance model, which does not include the diameter of CNTs as a parameter, is applicable to SW CNT networks, as shown in the supplementary material, section 1. For the same reason, our conductance model is applicable to the random networks of MW CNTs with small diameters ($d_{\mathrm{CNT}} < 5$ nm), because each individual nanotube in a small-diameter MW CNT behaves similarly to a SW CNT [13].

[5] The results obtained here cannot be directly applied to systems comprising semiconducting and metallic NWs, since NWs have a significantly higher junction conductance (two orders of magnitude [45–47]) and a considerably shorter mean free path (one order of magnitude [48]) than CNTs. However, the conductance model described here can be applied to systems of NWs using appropriate electrical characteristics of individual NWs and the junctions between them.

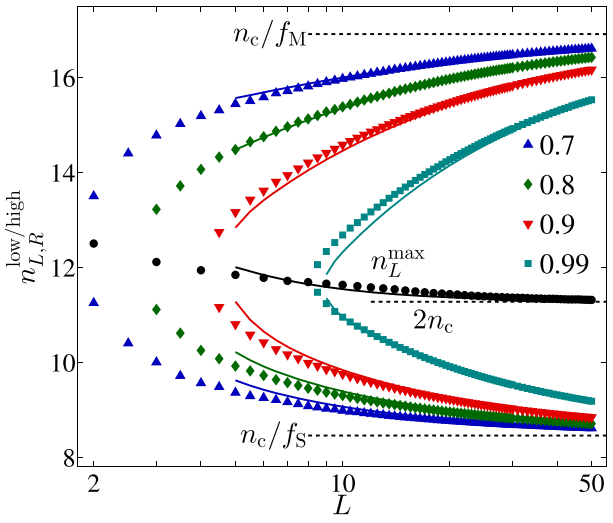

Figure 2. The dependence of the S$\overline{\text{M}}$-dominant region on the normalized system size L, for different tolerances $R = 0.7$, 0.8, 0.9, and 0.99. The points are the MC simulation results and the solid lines are obtained using our analytic model (see the supplementary material, section 2). With increasing system size L, the value of CNT density n_L^{max}, where the percolation probability through only s-CNT paths $R_{n,L}^{S\overline{M}}$ reaches its maximum, converges to $2n_c$, the low-bound density $n_{L,R}^{low}$ to n_c/f_S, and the high-bound density $n_{L,R}^{high}$ to n_c/f_M.

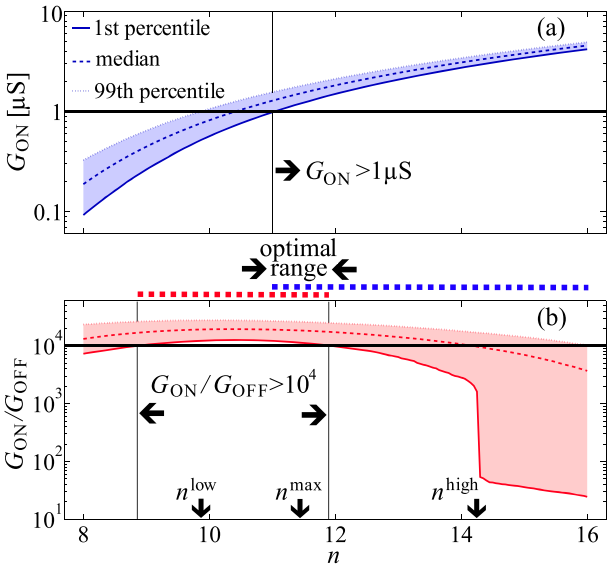

Figure 3. On-conductance G_{ON} (a) and on/off ratio G_{ON}/G_{OFF} (b) as a function of the normalized CNT density n for a symmetric TFT with the CNT length $l_{CNT} = 5$ μm and the channel size $L_{CH} = W_{CH} = 100$ μm, i.e. the normalized system size $L = 20$. The solid line represents the 1st percentile, while the dashed and dotted lines correspond to the median and 99th percentile, respectively, of the device population. The arrows denote regions where more than 99% of realized devices have: (a) on-conductance higher than 1 μS (horizontal bold line) or (b) an on/off ratio higher than 10^4 (horizontal bold line). The positions of the lower $n_{20,0.99}^{low}$ and higher $n_{20,0.99}^{high}$ bounds of 0.99 percolation probability for the S$\overline{\text{M}}$ regime are also given, as well as the position of S$\overline{\text{M}}$ probability maximum n_{20}^{max}.

on-conductance G_{ON} and resulting on-current I_{ON} are reduced by the presence of the low-conducting s-CNT/m-CNT junctions, see figure 1(a). At the same time, since an m-CNT path does not exist, off-conductance is low and therefore, the on/off ratio is high, see figures 1(a) and (b). The second operation regime (S$\overline{\text{M}}$) occurs for the medium CNT density ($n_c/f_S < n < n_c/f_M$) when only s-CNT paths exist, and the current flows through high-conducting s-CNT/s-CNT junctions resulting in a high on-current I_{ON}, see figure 1(c). However, the CNT density ($n = 12$) is still lower than the percolation threshold of only m-CNTs and the CNT TFT in the off-state is not short-circuited through an m-CNT path. Therefore, the CNT network can simultaneously achieve high on-conductance G_{ON} and a high on/off ratio G_{ON}/G_{OFF}, see figures 1(c) and (d). Finally, the third regime (M) of the CNT network according to the percolation characteristics occurs at densities close to and above the percolation threshold of only m-CNTs, i.e. n_c/f_M. For a high CNT density ($n = 16$) at least one m-CNT path exists and a high on-conductance is obtained, see figure 1(e). On the other hand, in the off-state the CNT network is shorted through the m-CNTs and, hence, the on/off ratio is very low, see figures 1(e) and (f). Therefore, the CNT network in the M operation regime cannot be used as an active medium for transistors with a high switching performance.

According to our recently determined parameters for moments of the percolation probability distribution function [28], we will determine a region of the CNT density n where s-CNT paths are dominant (S$\overline{\text{M}}$) and, therefore, the on-current and on/off ratio are expected to be high. Details of our analytic model for the percolation probability functions are given in the supplementary material, section 2. We define a density range with lower boundary $n_{L,R}^{low}$ and upper boundary $n_{L,R}^{high}$, where the probability of percolation only through s-CNT paths $R_{n,L}^{S\overline{M}}$ is higher than a relative number R ($0 \leqslant R \leqslant 1$), see the supplementary material, section 2. As one would expect, the range defined by $n_{L,R}^{high}$ and $n_{L,R}^{low}$ increases with the normalized system size L and decreases with R, see figure 2. We can further observe interesting features of the shape of the S$\overline{\text{M}}$ percolation density range with increasing system size: (i) the position of S$\overline{\text{M}}$ percolation probability maximum n_L^{max} converges to $2n_c$ with increasing system size, (ii) the low-bound density $n_{L,R}^{low}$ decreases and converges to the percolation threshold of s-CNT paths n_c/f_S, and (iii) the high-bound density $n_{L,R}^{high}$ increases and converges to the percolation threshold of m-CNT paths n_c/f_M, see figure 2.

In the rest of this section, we will quantify the dependence of the calculated on-conductance and on/off ratio on the CNT density, length, and system size. The aim of this paper is to restrict the ranges of these parameters for which acceptable transistor characteristics are obtained with a realization probability higher than 99%. For most kinds of integrated circuit applications the acceptable values for on-conductance and on/off ratio are 1 μS and 10^4, respectively [23, 37, 49].

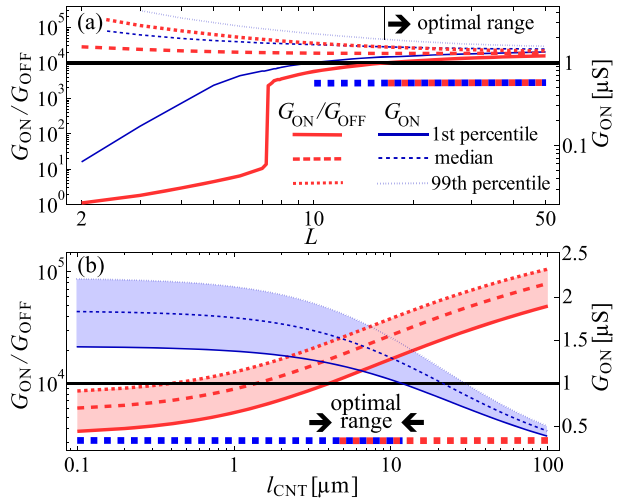

Figure 4. The dependence of on-conductance G_{ON} and the on/off ratio G_{ON}/G_{OFF} on (a) the normalized system size L for symmetric-channel TFTs with CNT length $l_{CNT} = 5$ μm and a normalized density equal to n_L^{max}, and (b) the CNT length l_{CNT} for a symmetric system with the normalized size $L = 20$ and a normalized CNT density n equal to $n_{20}^{max} = 11.45$. The solid lines represent the 1st percentile, while the dashed and dotted lines correspond to the median and 99th percentile, respectively, of the device population. The arrows denote regions where more than 99% of realized devices have on-conductance higher than 1 μS and an on/off ratio higher than 10^4 (horizontal bold lines).

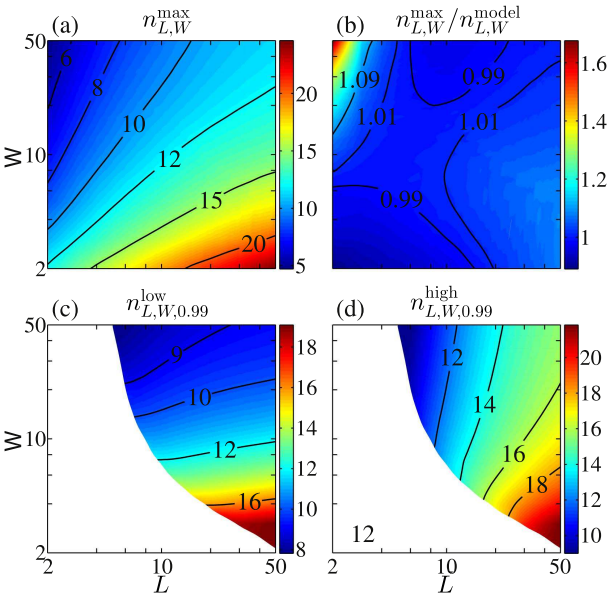

Figure 5. The dependence of (a) the normalized density $n_{L,W}^{max}$ where the probability of S$\overline{\text{M}}$ percolation reaches maximum and (b) the ratio between the MC simulation results $n_{L,W}^{max}$ on the values $n_{L,W}^{model}$ obtained using our analytic model (see the supplementary material, section 4) on the normalized channel width W and length L. The low-bound $n_{L,W,0.99}^{low}$ (c) and high-bound density $n_{L,W,0.99}^{high}$ (d) determine a density range where the probability of S$\overline{\text{M}}$ realizations is higher than 0.99.

The results are shown in figure 3 as a function of the CNT normalized density n for $l_{CNT} = 5$ μm and the system size $W_{CH} = L_{CH} = 100$ μm, i.e. the normalized system size $L = 20$. The on-conductance G_{ON} increases with CNT density n and the 1st and 99th percentiles converge to the median value, see figure 3(a). The difference between the 99th and 1st percentile of the on/off ratio G_{ON}/G_{OFF} reaches a minimum close to n_{20}^{max} and rapidly increases when the CNT density n becomes higher than $n_{20,0.99}^{high}$, see figure 3(b). For densities higher than $n_{20,0.99}^{high}$ the percolation probability of M configurations $R_{n,L}^{M}$ is higher than 1%, i.e. $R_{n,L}^{M} > 1\%$, and therefore the 1st-percentile realization belongs to the M regime and a sharp decrease in on/off behavior is obtained. One can observe that the maximum of the on/off ratio is between the densities $n_{20,0.99}^{low}$ and $n_{20,0.99}^{high}$. More than 99% of realized devices exhibit simultaneous on-conductance higher than 1 μS and an on/off ratio higher than 10^4 when the normalized density n is close to n_{20}^{max}, see figures 3(a) and (b).

A similar behavior of the on-conductance G_{ON} and on/off ratio G_{ON}/G_{OFF} can be observed in figure 4(a) with increasing the normalized system size L. While the percentiles of the on-conductance G_{ON} experience continuous convergence to the infinite system value, the on/off ratio exhibits a sharp transition in the 1st-percentile behavior at the normalized system size $L \approx 7$. For a system size below $L < 7$ the percolation probability of realizations through only m-CNTs is higher than 1%, i.e. $R_{n,L}^{M} > 1\%$, and therefore the 1st-percentile realization is short-circuited with $G_{ON}/G_{OFF} < 10$, see the supplementary material, section 3. On the other hand, more than 99% of realized devices exhibit simultaneous on-conductance higher than 1 μS and an on/off ratio higher than 10^4 when the normalized system size is $L > 16$, see figure 4(a).

The influence of CNT length l_{CNT} on the transistor performance is explored in figure 4(b). Here, the normalized system size is fixed and large, $L = 20$, in order to minimize the influence of finite-size scaling effects on the transistor performance, see [50]. Therefore, on-conductance G_{ON} and on/off ratio G_{ON}/G_{OFF} depend only on the electrical characteristics of individual nanotubes, i.e. their length l_{CNT}, in accordance with equation (1). When the CNT length l_{CNT} is larger than the electron mean free path, i.e. $l_{CNT} > 1$ μm, diffusive transport in CNTs becomes dominant and the on-conductance G_{ON} of the network starts to decrease linearly with the CNT length, see figure 4(b). At the same time, due to an increased resistance of m-CNTs, leak-currents in the off-state through the m-CNTs decrease and the on/off ratio improves with increasing CNT length, see figure 4(b). It is important to note that in this trade-off, the improvement of the on/off ratio is one order of magnitude with increasing l_{CNT} from 1 μm to 10 μm while G_{ON} decreases only 10%. However, more than 99% of realized devices exhibit simultaneously high on-conductance and a high on/off ratio when the CNT length is between $l_{CNT} = 4 - 12$ μm, see figure 4(b).

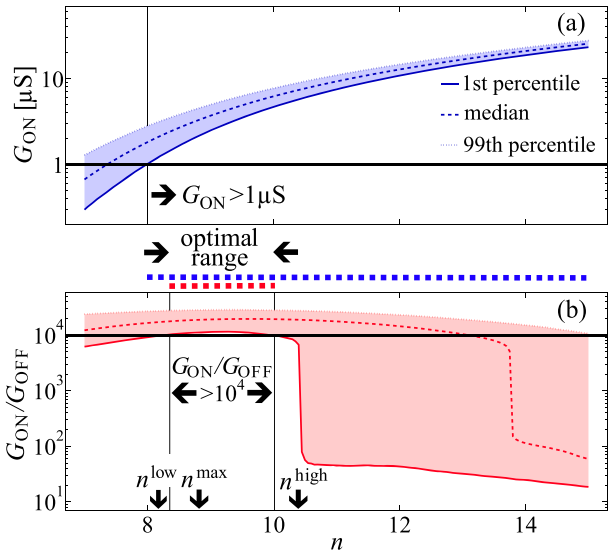

Figure 6. On-conductance G_{ON} (a) and on/off ratio G_{ON}/G_{OFF} (b) as a function of the normalized CNT density n for a narrow-channel TFT with the CNT length $l_{CNT} = 5$ μm and the channel dimensions $L_{CH} = 40$ μm and $W_{CH} = 250$ μm, i.e. the normalized system dimensions $L = 8$ and $W = 50$. The solid line represents the 1st percentile, while the dashed and dotted lines correspond to the median and 99th percentile, respectively, of the device population. The arrows denote regions where more than 99% of realized devices have: (a) on-conductance higher than 1 μS (horizontal bold line) or (b) on/off ratio higher than 10^4 (horizontal bold line). The positions of the lower $n^{low}_{8,50,0.99}$ and higher $n^{high}_{8,50,0.99}$ bounds of the 0.99 percolation probability for S$\overline{\text{M}}$ regime are also given, as well as the position of S$\overline{\text{M}}$ probability maximum $n^{max}_{8,50}$.

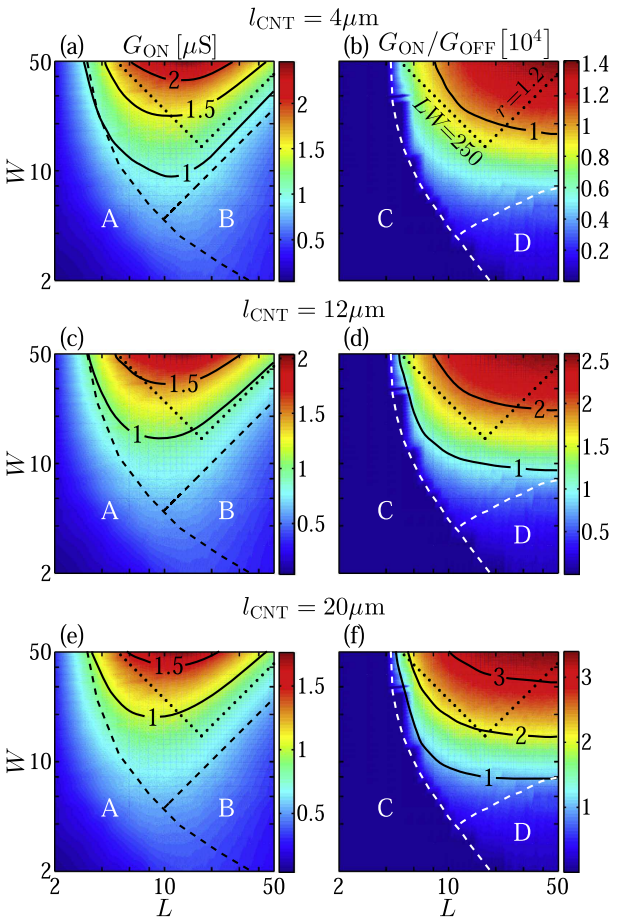

Figure 7. The results for the 1st percentile of the on-conductance G_{ON} ((a), (c), and (e)) and the on/off ratio G_{ON}/G_{OFF} ((b), (d), and (f)) calculated at $n^{max}_{L,W}$ as a function of the normalized channel width W and length L for different CNT lengths $l_{CNT} = 4$, 12, and 20 μm. Region A represents CNT TFT configurations with a probability of S$\overline{\text{M}}$ percolation higher than 1%, i.e. $R^{S\overline{M}}_{n,L,W} > 1\%$, while region B represents configurations with a high aspect ratio (here $r > 2$). TFTs in the C region feature networks with a probability of M percolation higher than 1%, i.e. $R^{M}_{n,L,W} > 1\%$, while the region D denotes networks with a high CNT density (here $n > 15$). The area above the dotted lines ($LW = 250$ and $L/W = 1.2$) can be used as an approximation of the region where the random CNT TFTs simultaneously attain high on-conductance and a high on/off ratio.

4. Asymmetric-channel results

For asymmetric-channel configurations the dependence of the normalized density where S$\overline{\text{M}}$ percolation probability reaches maximum $n^{max}_{L,W}$ on the normalized system dimensions L and W is shown in figure 5(a). The normalized density $n^{max}_{L,W}$ increases with increasing normalized channel length L and decreases with increasing width W, see figure 5(a). The agreement between the MC simulation results $n^{max}_{L,W}$ and the values $n^{model}_{L,W}$ obtained from our analytic model (see the supplementary material, section 4) is better than 1% for the systems with $L > 5$, see figure 5(b). From figures 5(c) and (d) we expect to achieve 99% only s-CNT conducting realizations roughly above the line $L_{CH}W_{CH} > 250\ l^2_{CNT}$. Within that region we see that $n^{low}_{L,W,0.99}$ primarily depends on the system width W. On the other hand, the upper limit of the 99% confidence region, $n^{high}_{L,W,0.99}$ depends on both the normalized length L and width W.

The random CNT TFTs with an asymmetric channel have similar characteristics of the on-conductance G_{ON} and on/off ratio G_{ON}/G_{OFF} compared to the symmetric-channel configurations, see figures 3 and 6. The on-conductance G_{ON} also increases with increasing CNT density n and the 1st and 99th percentiles converge to the median value, see figure 6(a). The difference between the 99th and 1st percentile of the on/off ratio G_{ON}/G_{OFF} also reaches its minimum close to the density where the probability of S$\overline{\text{M}}$ percolation reaches its maximum, i.e. $n^{max}_{8,50}$, and rapidly increases when the CNT density becomes higher than $n^{high}_{8,50,0.99}$, see figure 6(b). Similarly, the maximum of the on/off ratio is between densities $n^{low}_{8,50,0.99}$ and $n^{high}_{8,50,0.99}$, and more than 99% of realized devices exhibit simultaneously on-conductance higher than 1 μS and an on/off ratio higher than 10^4 when the normalized density n is close to $n^{max}_{8,50}$, see figures 6(a) and (b). Hence, the density $n^{max}_{L,W}$ for asymmetric, as well as symmetric, configurations can be used as a compromise value for obtaining the optimized

transistor performance, see figures 3 and 6. However, narrow-channel configurations generally have a higher on-conductance compared to symmetric channels[6]. Indeed, as can be seen from figures 3(a) and 6(a), a narrow-channel TFT with the aspect ratio $r = 8/50$ has roughly $1/r \approx 6$ times higher on-conductance G_{ON} compared to the symmetric-channel configuration with the same normalized channel size $\mathcal{L}$ and CNT length l_{CNT}.

The 1st percentiles of the on-conductance G_{ON} and on/off ratio G_{ON}/G_{OFF} are calculated for the same structural parameters L, W, and $n_{L,W}^{max}$, and different CNT lengths $l_{CNT} = 4$, 8, and 12 μm, see figure 7. In accordance with the results shown for the symmetric-channel configuration in figure 4(b) we note that with increasing CNT length l_{CNT} the on-conductance G_{ON} decreases, while the on/off ratio G_{ON}/G_{OFF} increases, see figure 7. When the CNT length l_{CNT} is below 4 μm ballistic electrical transport becomes dominant and the on/off ratio becomes lower than 10^4, see figures 7(b), (d), and (f). On the other hand, when l_{CNT} is higher than 20 μm, high on-conductance can be attained only for a very large channel with dimensions of the order of 1 mm, see figure 7(e). Hence, the CNT length in the range $l_{CNT} = 4 - 20$ μm results in an acceptable balance between the on-conductance and on/off performance of CNT TFTs.

Regions A and B in figure 7 represent the CNT networks with a low 1st-percentile value of the on-conductance G_{ON}. Region A is defined as a region where the probability of $\overline{S}\,\overline{M}$ percolation is higher than 1%, i.e. $R_{n,L,W}^{\overline{S}\,\overline{M}} > 1\%$, and therefore the 1st-percentile realization is a mixed path with low-conducting s-CNT/m-CNT junctions. The realizations in region B have a high value of the aspect ratio r and therefore a low overall on-conductance (see footnote 6). On the other hand, regions C and D in figure 7 represent the CNT networks with a low 1st-percentile value of the on/off ratio G_{ON}/G_{OFF}. The TFTs in region C feature networks with a probability of percolation through only m-CNTs higher than 1%, i.e. $R_{n,L,W}^{M} > 1\%$, and therefore the 1st-percentile realization is short-circuited having a very low G_{ON}/G_{OFF}. The networks operating in the D region are not short-circuited but the on/off ratio is low because of high leak-currents in off-state through the high-density m-CNTs. We can conclude that the optimal dimensions of the CNT TFT channel regarding the device switching performance are those outside the regions A, B, C, and D shown in figure 7. The dotted lines approximate the region where CNT TFTs attain high on-conductance and, at the same time, a high on/off ratio. Therefore, the random CNT TFTs with a channel aspect ratio $L_{CH}/W_{CH} < 1.2$ and a normalized size $L_{CH}W_{CH}/l_{CNT}^2 > 250$ with a probability higher than 99% exhibit on-conductance higher than 1 μS and, at the same time, an on/off ratio higher than 10^4.

[6] The on-conductance of a rectangular TFT channel is $G_{ON} = \sigma_{ON}W_{CH}/L_{CH} = \sigma_{ON}/r$, and similarly the off-conductance is $G_{OFF} = \sigma_{OFF}/r$, where σ_{ON} and σ_{OFF} are the on- and off-state conductivities, respectively. As one can see, the on-conductance G_{ON} is inversely proportional to the aspect ratio r, while the on/off ratio $G_{ON}/G_{OFF} = \sigma_{ON}/\sigma_{OFF}$ is independent of r.

5. Conclusions

In this paper, we present numerical simulation results for the switching performance of transistors based on random networks of as-grown CNTs. The CNT thin films studied here are considered a suitable material for low-cost, flexible, and transparent TFTs. One factor that makes CNT films complex is that they contain both metallic and semiconducting nanotubes. Only the s-CNTs have highly modulated conductance by the gate and only junctions between CNTs of the same type are highly conductive. Therefore, the random CNT TFTs that percolate through only s-CNT paths can simultaneously attain high on-conductance and a high on/off ratio. As a result, a key limitation in scaling up the production of random CNT TFTs with a high on-current and on/off ratio is a requirement to achieve uniform performance of the realized devices.

We determine the probabilities of different conduction regimes for as-grown CNT networks and derive expressions which represent an excellent fit to the data calculated using numerical simulations. We also show that the fraction of 1:2 of metallic to semiconducting nanotubes provides sufficient design freedom. We avoid creating m-CNT paths, while at the same time determine a density range where the rate of realizations that percolate only through s-CNT paths is higher than 99%. Since there is a trade-off between the on-conductance and on/off ratio regarding the CNT density, we show that the position of the only s-CNT percolation probability maximum can be used as a good balance for the CNT density value. In the CNT conductance model we have included diffusive electrical transport through CNTs typical for rodlike nanostructures whose length is larger than the mean free path of the electrons. This enables us to consider the influence of the CNT length on the device characteristics. When the CNT length increases, diffusive transport in the CNTs becomes dominant and on-conductance decreases with CNT length. At the same time, because of the increased resistance of m-CNTs, the leak-currents in the off-state through the m-CNTs decrease and the on/off ratio improves. This results in a further trade-off, however, the improvement of the on/off ratio is much larger than the detrimental loss of the on-conductance.

Asymmetric systems have lower finite-size scaling exponents than symmetric systems. This results in more pronounced finite-size scaling behavior than in the symmetric case and enables us even more design freedom. We performed a parameter study to find the optimal channel dimensions for CNT TFTs. We present a region of the channel dimensions where most of the random CNT realizations have satisfactory transistor performance. According to the criteria of high on-conductance at the same time as a high on/off ratio, within the 99% confidence range, the optimal region of the channel dimensions can be estimated with aspect ratio $L_{CH}/W_{CH} < 1.2$ and size $L_{CH}W_{CH}/l_{CNT}^2 > 250$. This conclusion remains valid when the CNT length belongs to the range $l_{CNT} = 4 - 20$ μm, resulting in an acceptable balance between the on-conductance and on/off performance of the

random CNT TFTs. We have also demonstrated that the on-conductance and on/off ratio results obtained using our conductance model show excellent agreement with recently published experimental results. Hence, we conclude that the channel dimensions L_{CH} and W_{CH}, CNT length l_{CNT}, and density n are the only parameters needed for the description and optimization of transport processes in TFTs based on random networks of as-grown CNTs.

Acknowledgments

This work was supported by the Ministry of Education, Science, and Technological Development of the Republic of Serbia under projects ON171017 and III45018. Numerical simulations were run on the PARADOX supercomputing facility at the Scientific Computing Laboratory of the Institute of Physics Belgrade. MŽ thanks Dr. Nenad Vukmirović of the Institute of Physics Belgrade for valuable discussions.

References

[1] Cao Q, Kim H-S, Pimparkar N, Kulkarni J P, Wang C, Shim M, Roy K, Alam M A and Rogers J A 2008 *Nature* **454** 495
[2] De Volder M F L, Tawfick S H, Baughman R H and Hart A J 2013 *Science* **339** 535
[3] Abdelhalim A, Abdellah A, Scarpa G and Lugli P 2014 *Nanotechnology* **25** 055208
[4] Bartolomeo A D, Rinzan M, Boyd A K, Yang Y, Guadagno L, Giubileo F and Barbara P 2010 *Nanotechnology* **21** 115204
[5] Engel M, Small J P, Steiner M, Freitag M, Green A A, Hersam M C and Avouris P 2008 *ACS Nano* **2** 2445
[6] Sun D-M, Timmermans M Y, Tian Y, Nasibulin A G, Kauppinen E I, Kishimoto S, Mizutani T and Ohno Y 2011 *Nat. Nanotechnol.* **6** 156
[7] Chandra B, Park H, Maarouf A, Martyna G J and Tulevski G S 2011 *Appl. Phys. Lett.* **99** 072110
[8] Wang C, Chien J-C, Takei K, Takahashi T, Nah J, Niknejad A M and Javey A 2012 *Nano Lett.* **12** 1527
[9] Park S, Vosguerichian M and Bao Z 2013 *Nanoscale* **5** 1727
[10] Lau P H, Takei K, Wang C, Ju Y, Kim J, Yu Z, Takahashi T, Cho G and Javey A 2013 *Nano Lett.* **13** 3864
[11] Che Y, Chen H, Gui H, Liu J, Liu B and Zhou C 2014 *Semicond. Sci. Technol.* **29** 073001
[12] Liu N, Yun K N, Yu H-Y, Shim J H and Lee C J 2015 *Appl. Phys. Lett.* **106** 103106
[13] Li J and Pandey G P 2015 *Annu. Rev. Phys. Chem.* **66** 331
[14] Zaumseil J 2015 *Semicond. Sci. Technol.* **30** 074001
[15] Kumar S, Pimparkar N, Murthy J Y and Alam M A 2006 *Appl. Phys. Lett.* **88** 123505
[16] Kocabas C, Pimparkar N, Yesilyurt O, Kang S J, Alam M A and Rogers J A 2007 *Nano Lett.* **7** 1195
[17] Rouhi N, Jain D and Burke P J 2011 *ACS Nano* **5** 8471
[18] Sangwan V K, Behnam A, Ballarotto V W, Fuhrer M S, Ural A and Wiliams E D 2010 *Appl. Phys. Lett.* **97** 043111
[19] Collins P G, Arnold M S and Avouris P 2001 *Science* **292** 706
[20] Arnold M S, Green A A, Hulvat J F, Stupp S I and Hersam M C 2006 *Nat. Nanotechnol.* **1** 60
[21] Zhang G, Qi P, Wang X, Lu Y, Li X, Tu R, Bangsaruntip S, Mann D, Zhang L and Dai H 2006 *Science* **314** 974
[22] Kumar S, Cola B A, Jackson R and Graham S 2011 *J. Elect. Packaging* **133** 020906
[23] Hu L, Hecht D S and Grüner G 2010 *Chem. Rev.* **110** 5790
[24] Hecht D S, Hu L and Irvin G 2011 *Adv. Mater.* **23** 1482
[25] Snow E S, Novak J P, Campbell P M and Park D 2003 *Appl. Phys. Lett.* **82** 2145
[26] Li J, Zhang Z-B and Zhang S-L 2007 *Appl. Phys. Lett.* **91** 253127
[27] Seppälä S, Häkkinen E, Alava M J, Ermolov V and Seppälä E T 2010 *Europhys. Lett.* **91** 47002
[28] Žeželj M, Stanković I and Belić A 2012 *Phys. Rev.* E **85** 021101
[29] Žeželj M and Stanković I 2012 *Phys. Rev.* B **86** 134202
[30] Stanković I, Kröger M and Hess S 2002 *Comput. Physics Commun.* **145** 371
[31] Balaž A, Vidanović I, Stojiljković D, Vudragović D, Belić A and Bogojević A 2012 *Commun. Comput. Phys.* **11** 739
[32] Heitz J, Leroy Y, Hébrard L and Lallement C 2011 *Nanotechnology* **22** 345703
[33] Fuhrer M S *et al* 2000 *Science* **288** 494
[34] Stauffer D and Aharony A 2003 *Introduction to Percolation Theory* 2nd edn (London: Taylor and Francis)
[35] Behnam A and Ural A 2007 *Phys. Rev.* B **75** 125432
[36] Javey A, Guo J, Paulsson M, Wang Q, Mann D, Lundstrom M and Dai H 2004 *Phys. Rev. Lett.* **92** 106804
[37] Avouris P 2004 *MRS Bull.* **29** 403
[38] Purewal M S, Hong B H, Ravi A, Chandra B, Hone J and Kim P 2007 *Phys. Rev. Lett.* **98** 186808
[39] Bachtold A, Hadley P, Nakanishi T and Dekker C 2001 *Science* **294** 1317
[40] Javey A, Guo J, Wang Q, Lundstrom M and Dai H 2003 *Nature* **424** 654
[41] Park J-Y, Rosenblatt S, Yaish Y, Sazonova V, Üstünel H, Braig S, Arias T A, Brouwer P W and McEuen P L 2004 *Nano Lett.* **4** 517
[42] Franklin A D and Chen Z 2010 *Nat. Nanotechnol.* **5** 858
[43] Buldum A and Lu J P 2001 *Phys. Rev.* B **63** 161403
[44] Sarker B K, Kang N and Khondaker S I 2014 *Nanoscale* **6** 4896
[45] Mutiso R M, Sherrott M C, Rathmell A R, Wiley B J and Winey K I 2013 *ACS Nano* **7** 7654
[46] Langley D P, Giusti G, Lagrange M, Collins R, Jiménez C, Bréchet Y and Bellet D 2014 *Sol. Energy Mater. Sol. Cells* **125** 318
[47] Bellew A T, Manning H G, Gomes da Rocha C, Ferreira M S and Boland J J 2015 *ACS Nano* **9** 11422
[48] Bid A, Bora A and Raychaudhuri A K 2006 *Phys. Rev.* B **74** 035426
[49] Wang C, Zhang J and Zhou C 2010 *ACS Nano* **4** 7123
[50] Kuwahara Y, Nihey F, Ohmori S and Saito T 2015 *Carbon* **91** 370